Numerically Efficient Modeling of CNT Transistors With Ballistic and Nonballistic Effects for Circuit Simulation

Tom J. Kazmierski, *Member, IEEE*, Dafeng Zhou, Bashir M. Al-Hashimi, *Fellow, IEEE*, and Peter Ashburn, *Member, IEEE*

***Abstract*—This paper presents an efficient carbon nanotube (CNT) transistor modeling technique that is based on cubic spline approximation of the nonequilibrium mobile charge density. The approximation facilitates the solution of the self-consistent voltage equation in a CNT so that calculation of the CNT drain–source current is accelerated by at least two orders of magnitude. A salient feature of the proposed technique is its ability to incorporate both ballistic and nonballistic transport effects without a significant computational cost. The proposed models have been extensively validated against reported CNT ballistic and nonballistic transport theories and experimental results.**

***Index Terms*—Carbon nanotube (CNT) transistors, circuit simulation, nonballistic effects, numerical modeling.**

I. Introduction

CARBON nanotube (CNT) transistors have been demonstrated to have potential of becoming an attractive solution in addition to their silicon counterparts, mainly due to their electrostatic properties, such as ballistic or near-ballistic transport of electrons and very low conduction threshold voltages [1]–[3], which make CNTs suitable for ultrahigh-speed and ultralow-power circuit design. While physical properties of CNTs are studied in greater depth and the theory of CNTs becomes better understood, most state-of-the-art physical and circuit-level models are currently concerning ballistic or near-ballistic transport [1], [4]–[12]. There is a growing need for numerically efficient CNT models suitable for implementation in circuit-level simulators, especially in the light of the recently reported successful implementations of logic circuits built with CNTs [13]. Very recently, breakthrough improvements to accurate SPICE-compatible CNT transistor modeling have been proposed where not only the ballistic transport but also a number of nonballistic effects have been included [11], [12]. However, the main stumbling block in the development of a circuit-level model is the fact that accurate calculation of the mobile charge involves numerical integration of the densities of states over the number of allowed energy levels using the Fermi probability distribution. In addition, as the total drain current is affected not only by the nonequilibrium mobile charge in the nanotube but also by the charges present at terminal capacitances, the solution of an implicit nonlinear algebraic equation is necessary using some iterative approach, such as the Newton–Raphson method [1], [6]. Resulting CPU times are prohibitive for the purpose of circuit simulation where networks involving large numbers of such devices may need to be analyzed. For example, the MATLAB script named FETToy [14] available online as a reference implementation of the state-of-the art ballistic CNT theory, requires more than 12 s of the CPU time on a Pentium IV PC to calculate a family of current drain characteristics for a single transistor [15]. Inclusion of nonballistic effects aggravates the problem of excessive CPU time consumption.

It has been recently proposed to eliminate the need for costly Newton–Raphson iterations and the numerical evaluation of the Fermi–Dirac integral while still maintaining a good agreement with the physical theory [8], [16]. These techniques are based on piecewise approximation of the charge density profiles, either linear [8] or nonlinear [16], to simplify calculations. In this paper, we investigate the use of a cubic spline approximation of the charge density that, like the piecewise nonlinear approximation, also allows a closed-form solution of the self-consistent voltage equation. The main advantage of using cubic splines is an improved control of the approximation accuracy. Furthermore, as some theories on the nonballistic effects have recently emerged [11], [12], [17]–[21], in addition to the ballistic transport model [16], we demonstrate how the proposed approximation can be applied to include nonballistic behavior.

The approach presented in this paper addresses the need for efficient calculation of the $I_{\rm DS}$ current resulting from ballistic and nonballistic transport in the CNT itself. To develop a complete CNT transistor model, a number of additional effects representing nonidealities and parasitics, such as contact effects or series resistances, which are external to the inner CNT transistor, also need to be considered.

II. Mobile Charge Density and Self-Consistent Voltage

When an electric field is applied between the drain and the source of a CNT transistor, as illustrated in Fig. 1, a nonequilibrium mobile charge is induced in the nanotube [1], [22], [23]

$$\Delta Q = q(N_S + N_D - N_0) \tag{1}$$

Manuscript received August 9, 2008; revised January 14, 2009. First published March 10, 2009; current version published January 8, 2010. This work was supported by the Engineering and Physical Sciences Research Council (EPSRC), U.K., under Grant EP/E035965/1. The review of this paper was arranged by Associate Editor C. Zhou.

The authors are with the School of Electronics and Computer Science, University of Southampton, Southampton, SO17 1BJ, U.K. (e-mail: tjk@ecs.soton.ac.uk; dz05r@ecs.soton.ac.uk; bmah@ecs.soton.ac.uk; pa@ecs.soton.ac.uk).

Digital Object Identifier 10.1109/TNANO.2009.2017019

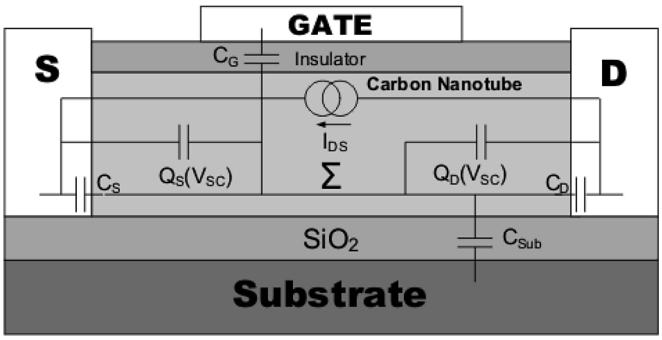

Fig. 1. Structure layout of a top-gate CNT transistor showing components of the proposed equivalent circuit model with the virtual node Σ for $V_{\rm SC}$.

where N_S is the density of positive velocity states filled by the source, N_D is the density of negative velocity states filled by the drain, and N_0 is the equilibrium electron density. These densities are determined by the Fermi–Dirac probability distribution as follows:

$$N_S = \frac{1}{2}\int_{-\infty}^{+\infty} D(E) f(E - U_{\rm SF}) dE \tag{2}$$

$$N_D = \frac{1}{2}\int_{-\infty}^{+\infty} D(E) f(E - U_{\rm DF}) dE \tag{3}$$

$$N_0 = \int_{-\infty}^{+\infty} D(E) f(E - E_F) dE \tag{4}$$

where $D(E)$, $U_{\rm SF}$, and $U_{\rm DF}$ are defined as

$$D(E) = D_0 \frac{E}{\sqrt{E^2 - (E_g/2)^2}} \Theta(E - E_g/2) \tag{5}$$

$$U_{\rm SF} = E_F - qV_{\rm SC} \tag{6}$$

$$U_{\rm DF} = E_F - qV_{\rm SC} - qV_{\rm DS} \tag{7}$$

where $D(E)$ is the density of states at the channel, $D_0 = 8/(3\pi V_{cc} a_{cc})$ is the constant density of states of a metallic nanotube, and E_g is the bandgap that can be calculated using $2a_{cc}V_{cc}/d$ [14], where a_{cc} and V_{cc} are the carbon π–π nearest-neighbor bond length and energy of the tight bonding model, respectively. $\Theta(E - E_g/2)$ equals 1 when $E > E_g/2$ and 0 when $E \leq E_g/2$.

$V_{\rm SC}$ is the self-consistent voltage, a recently introduced concept [1] that illustrates that the CNT energy band is affected by external terminal voltages, $D(E)$ is the density of states, E_F is the Fermi level, f is the Fermi probability distribution, q is the electronic charge, and E represents the energy levels per nanotube unit length. The self-consistent voltage $V_{\rm SC}$ is implicitly related to the device terminal voltages and charges at terminal capacitances by the following nonlinear algebraic equation [1], [8]:

$$V_{\rm SC} = \frac{-Q_t + qN_S(V_{\rm SC}) + qN_D(V_{\rm SC}) - qN_0}{C_\Sigma} \tag{8}$$

where Q_t represents the charge stored in terminal capacitances, and is defined as

$$Q_t = V_G C_G + V_D C_D + V_S C_S + V_{\rm Sub} C_{\rm Sub} \tag{9}$$

where C_G, C_D, C_S, and $C_{\rm Sub}$ are the gate, drain, source, and substrate capacitances, respectively, and the total terminal capacitance C_Σ is

$$C_\Sigma = C_G + C_D + C_S + C_{\rm Sub} \tag{10}$$

$$C_{\rm ox} = \frac{2\pi k_1 \varepsilon_0}{\ln\left((2t_{\rm ox} + d)/d\right)} \tag{11}$$

$$C_{\rm Sub} = \frac{2\pi k_2 \varepsilon_0}{\ln(4H_{\rm Sub}/d)} \tag{12}$$

where d is the diameter of the CNT, $H_{\rm Sub}$ is the thickness of the SiO_2 layer on the substrate, $t_{\rm ox}$ is the thickness of the gate insulator, and k_1 and k_2 are the relative permittivities of the gate and the substrate, respectively [24]. Meanwhile, the capacitances between terminals can be obtained as follows, as reported previously [14]:

$$C_G = C_{\rm ox} \tag{13}$$

$$C_S = 0.097 C_{\rm ox} \tag{14}$$

$$C_D = 0.040 C_{\rm ox}. \tag{15}$$

And the addition of $C_{\rm Sub}$ also implies that the body effects may be taken into account in further work. The standard approach to the solution of (8) is to use the Newton–Raphson iterative method, and in each iteration evaluate the integrals in (3) and (4) to obtain the state densities N_D and N_S.

III. Circuit Model and Spline-Based Approximation of Charge Densities

In an earlier work [15], we proposed to apportion equal parts of the equilibrium mobile charge density N_0 to the drain and source. This facilitates circuit implementation of the model because now the corresponding nonequilibrium mobile charge densities Q_S and Q_D can be modeled as nonlinear circuit capacitances, dependent on the self-consistent voltage $V_{\rm SC}$, and connected between a conceptual inner node, which represents the self-consistent potential, and CNT terminal nodes

$$Q_S(V_{\rm SC}) = q\left(N_S(V_{\rm SC}) - \frac{1}{2}N_0\right) \tag{16}$$

and

$$Q_D(V_{\rm SC}) = q\left(N_D(V_{\rm SC}) - \frac{1}{2}N_0\right). \tag{17}$$

The resulting equivalent circuit is shown in Fig. 2, where Σ is the hypothetical inner node described before, which comprises all the CNT charges. The current I_t represents the tunneling, one of the nonballistic effects discussed in Section IV. $I_{\rm DS}$ is the transport current determined by the self-consistent voltage $V_{\rm SC}$. If only ballistic transport is considered, $I_{\rm DS}$ is equivalent to current $I_{{\rm DS}_B}$ given by (18) next. In Section IV, we consider models of nonballistic effects that allow a more accurate representation of the transport current $I_{\rm DS}$.

According to the ballistic CNT ballistic transport theory [1], [14], the drain current caused by the transport of the nonequilibrium charge across the nanotube can be calculated using the

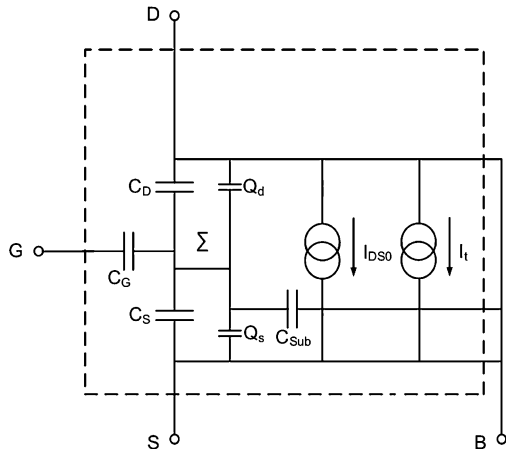

Fig. 2. Equivalent circuit for the proposed CNT transistor model.

Fermi–Dirac statistics as follows:

$$I_{\mathrm{DS}_0} = \frac{2qkT}{\pi\hbar}\left[\mathcal{F}_0\left(\frac{U_{\mathrm{SF}}}{kT}\right) - \mathcal{F}_0\left(\frac{U_{\mathrm{DF}}}{kT}\right)\right] \tag{18}$$

where $\mathcal{F}_0$ represents the Fermi–Dirac integral of order 0, k is Boltzmann's constant, T is the temperature, and $\hbar$ is reduced Planck's constant.

If the self-consistent voltage V_{SC} is known, the evaluation of the drain current poses no numerical difficulty as energy levels U_{SF} and U_{DF} can be found quickly from (6), (7), and I_{DS} calculated directly using the closed-form analytical solution of the Fermi–Dirac integral of order zero [25]. However, as it has already been highlighted before, the solution of the self-consistent voltage (8) is very time-consuming because it involves a Newton–Raphson iterative process in which each iteration requires numerical integration to obtain state densities $N_D(V_{\mathrm{SC}})$ and $N_D(V_{\mathrm{SC}})$. This is the main drawback of general methods in calculating charge densities. The next section outlines a piecewise approximation technique that eliminates the need for these complex calculations while maintaining a high modeling accuracy.

Our earlier work [16] proposed a piecewise nonlinear approximation technique that eliminates the need for these complex calculations. Although the piecewise nonlinear approach was demonstrated to be very fast and accurate in the transistor modeling, it requires a complex fitting process when deciding on the number of approximation pieces and intervals of the ranges, which makes this type of modeling inflexible. To improve the ease of use of the model without losing much of the computational efficiency, a piecewise approximation of the mobile charge based on cubic splines [26] can be used as an alternative. While cubic splines are generally cumbersome to apply in semiconductor modeling where multidimensional approximations are usually required, here they are particularly suitable and easy to apply because the dependence of nonequilibrium mobile charge on the self-consistence voltage is 1-D. As illustrated next, the numerical efficiency of the ballistic CNT transport model hinges on an efficient calculation of the nonequilibrium mobile charge. For the charge density defined in Section II

$$Q(V_{\mathrm{SC}}) = \frac{q}{2}\int_{-\infty}^{+\infty} D(E)f(E - E_F - V_{\mathrm{SC}})dE \tag{19}$$

a simple spline structure can be build, using n equally spaced points, to approximate the mobile charge dependence on V_{SC} using cubic polynomial pieces of the following form:

$$Q(V_{\mathrm{SC}}) = a_i V_{\mathrm{SC}}^3 + b_i V_{\mathrm{SC}}^2 + c_i V_{\mathrm{SC}} + d_i \tag{20}$$

where a_i, b_i, c_i, and d_i, $i = 1, \ldots, n-1$ are spline coefficients. This enables a closed-form solution of the self-consistent voltage (8) as, for each piece, it now becomes a polynomial equation of the third order. Thus, the need for costly Newton–Raphson iterations and evaluations of Fermi–Dirac integrals is eliminated.

IV. Nonballistic Transport Effects

Research into nonballistic transport in CNTs has recently yielded results, and some new theories have been reported. Studies of the energy domain reveal that the incommensurate system within a nonideal nanotube implies the existence of a general nonballistic regime [17]. The transport type in CNTs, ballistic or nonballistic, depends on the energy region. Studies of the energy domain reveal that the incommensurate system within a nonideal nanotube implies the existence of a general nonballistic regime [17]. For a CNT transistor with the length smaller than the carrier mean free path (MFP) but larger than the Coulomb blockade length, the ballistic transport will dominate. To travel through a single-defect Coulomb potential, the transmission coefficient can be calculated by $T_{\mathrm{defect}}(E) = G_{\mathrm{filled}}(E)/G_{\mathrm{empty}}(E)$ [18], where E is the energy of the hole in a nanotube. Therefore, the charging and discharging decides the maximum differential conductance through single transport channels, and E is directly determined by the terminal voltage V_{DS}. For nonballistic CNTs, this transmission coefficient fluctuation could be caused by mobility fluctuation. However, under the effects of scattering, E is much smaller than $\mathrm{q}V_{\mathrm{DS}}$ in the case. It has also been shown that a mismatch of helicity between adjacent shells may result in a short MFP [19]. In addition, all kinds of likely defects, such as vacancies, contamination, contact to the substrate, and adsorbed molecules, may cause nonballistic transport [19]. In the light of these results, the nonballistic transport in CNTs is likely to attract more research attention in the near future. Next, we outline four major nonballistic effects that have been implemented in our numerical models.

A. Elastic Scattering

The elastic scattering mechanism in the CNT channel region affects the channel resistance, and therefore makes a potential drop of the channel voltage. Assuming that MFP l_{eff} is proportional to the diameter of the nanotube [27], [28], which is $l_{\mathrm{eff}} = d/(d_0)\lambda_{\mathrm{eff}}$, where d_0 is the reference diameter when λ_{eff} is the elastic scattering MFP [12], and the transmission probability in the elastic scattering channel region can be expressed using $T_{\mathrm{eff}} = l_{\mathrm{eff}}/(L + l_{\mathrm{eff}})$, where d is the CNT diameter, $\lambda_{\mathrm{eff}} \approx 200$ nm [29], and L is the channel length. The

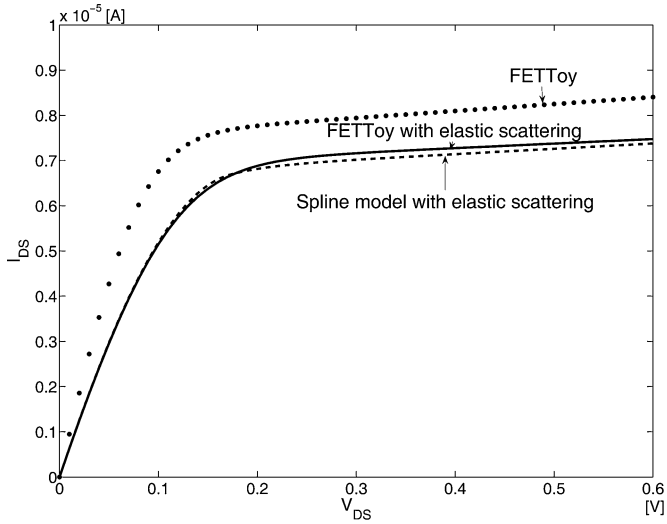

Fig. 3. Comparison of the drain currents at $V_G = 0.6$ V, $T = 300$ K, $E_F = -0.32$ eV, and $L = 300$ nm for models with the elastic scattering effect: FETToy model (dotted line), the FETToy-plus model (solid line), and the proposed spline Model 1 with the elastic scattering effect (dashed line).

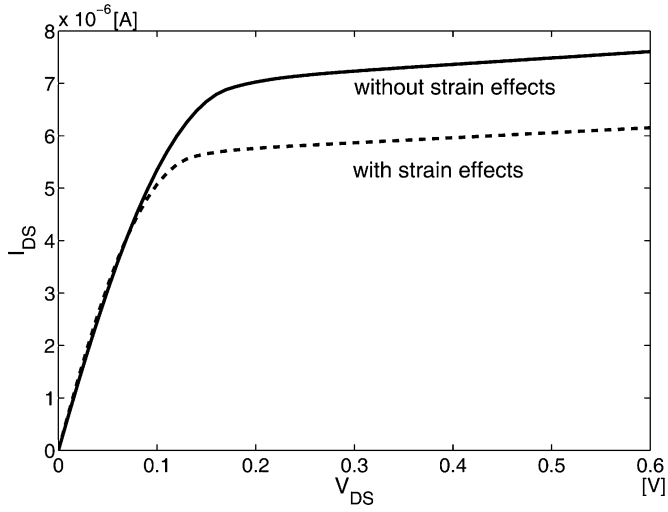

Fig. 4. Comparison of the drain currents at $V_G = 0.6$ V for models with (dashed line) and without (solid line) strain effects for a 300 nm long CNT channel with the diameter of 1 nm at $E_F = -0.32$ eV and $T = 300$ K.

channel potential drop can hereby be derived as

$$V_{\mathrm{DSeff}} = \frac{L}{L + (d/d_0)\lambda_{\mathrm{eff}}} V_{\mathrm{DS}}. \tag{21}$$

The contribution to the device current characteristics can be computed directly from the variable voltage V_{DSeff} due to the elastic scattering instead of the channel resistance, which simplifies the calculation efficiently [12]. Fig. 3 illustrates how the drain current changes when the elastic scattering effect relating to the channel length is considered.

B. Bandgap Tuning With Strain

It has been demonstrated that the transport property of a CNT can vary under strain [30]. Measurements have shown that the strain exerted onto a nanotube can change the bandgap, and thus affect the transport characteristics. The shape distortion formed by the strain can be treated as a key factor when calculating the extra bandgap caused by the effect

$$E_{g\mathrm{eff}} = E_g + \frac{dE_{g\mathrm{strain}}}{d\chi}\chi \tag{22}$$

where $E_{g\mathrm{eff}}$ is the effective bandgap under strain, $dE_{g\mathrm{strain}}$ is the gap shift due to the strain, and χ is defined as the distortion factor under strain.

It has also been indicated that the change rate of the bandgap $dE_{g\mathrm{strain}}/d\chi$ in the light of strain is chirality dependent, which can be computed using

$$\frac{dE_{g\mathrm{strain}}}{d\chi} = 3\sigma(1 + r_0)\mathrm{sign}(2p + 1)\cos(3\phi) \tag{23}$$

where σ is the overlap integral of the tight-binding C–C model, with a value of circa 2.7 eV, $r_0 \approx 0.2$ is the Poisson's ratio, ϕ is the chiral angle of the nanotube, and p comes from the CNT chirality: for a CNT with the chirality (m, n), $m - n = 3l + p$, where l and p are both integrals. It is indicated that the chirality and strain can both influence the bandgap of a CNT, and the total gap $E_{g\mathrm{eff}}$ could be either larger or lesser than the ideal diameter-based calculation E_g, which might cause the transport to decrease or increase, respectively.

Fig. 4 illustrates that when under certain strain conditions ($\chi = 0.1$, $p = 1$, and $\phi = 20°$), the drain current has been reduced due to the bandgap variation.

C. Tunneling Effect

The tunneling effect is also inevitable in the subthreshold region, which may cause self-consistence potential lowering, and thereby worsen the threshold characteristics of the transistor. One simplified method to describe the tunneling effect is to introduce a parameter T_t, called the tunneling probability [11], which is calculated as

$$T_t \approx \frac{\pi^2}{9} e^{-(\pi\sqrt{m^* E_g^3}/\sqrt{8}q\hbar F)} \tag{24}$$

where F is a parameter that triggers the tunneling under high electrical field [11] and m^* is the effective electron mass [11]. The tunneling current can then be obtained by T_t timing the maximum possible tunneling current using

$$I_t = \frac{4qkT}{h} T_t \sum_{m=1}^{M} [\ln(1 + e^{(qV_{\mathrm{DSeff}} - E_{g\mathrm{eff}}/2 - E_F)/K_B T}) - \ln(1 + e^{(qV_{\mathrm{DSeff}} - E_F)/K_B T})] \frac{\max(qV_{\mathrm{DSeff}} - E_{g\mathrm{eff}}, 0)}{qV_{\mathrm{DSeff}} - E_{g\mathrm{eff}}}. \tag{25}$$

It can be noted from Fig. 5 that the tunneling current has increased the total drain current throughout the V_{DS} range, but the effect only becomes obvious when the bias voltage is getting large and exceed a certain turning point depending on the coefficients.

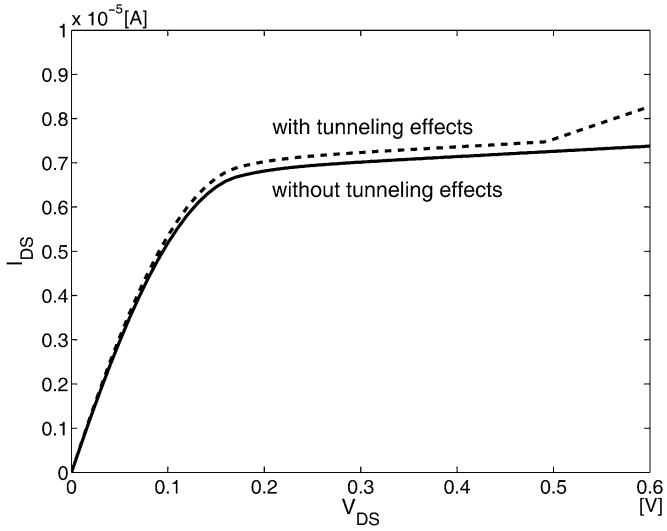

Fig. 5. Comparison of the drain currents at $V_G = 0.6$ V for models with (circlet line) and without (solid line) tunneling effects for a 300-nm-long CNT channel with the diameter of 1 nm at $E_F = -0.32$ eV and $T = 300$ K.

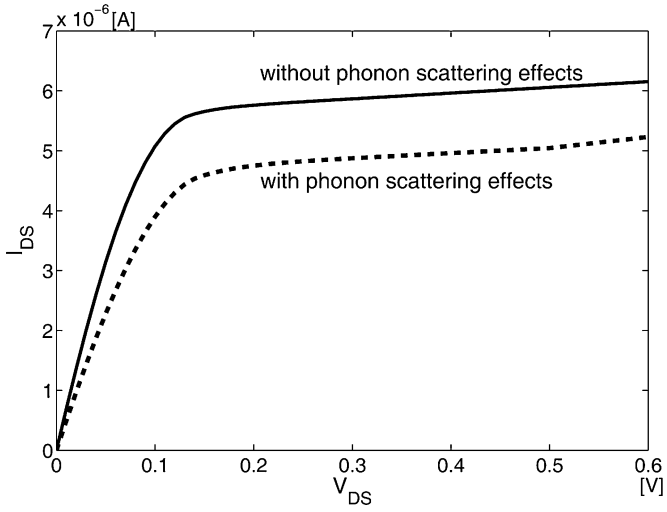

Fig. 6. Comparison of the drain currents at $V_G = 0.6$ V for models with (dashed line) and without (solid line) phonon scattering effects for a 300-nm-long CNT channel with the diameter of 1 nm at $E_F = -0.32$ eV and $T = 300$ K.

D. Phonon Scattering

For semiconducting CNTs, the scattering effects are related to the band energy. The effective phonon scattering MFP in a semiconducting nanotube can be computed by

$$\frac{1}{l_{\rm sc}(V_x)} = \frac{1}{l_{\rm ap}}\left[1 - \frac{1}{1+e^{(E_F - qV_{\rm SC} + qV_x)/K_BT}}\right] + \frac{1}{l_{\rm op}}\left[1 - \frac{1}{1+e^{(E_F - qV_{\rm SC} - \hbar\omega_{\rm op} + qV_x)/K_BT}}\right] \quad (26)$$

where $l_{\rm ap} = 500$ nm is a typical acoustic phonon scattering MFP value while $l_{\rm op} = 15$ nm is a typical optical phonon (OP) scattering MFP and $\hbar\omega_{\rm op} \approx 0.16$ eV is a typical OP energy [20], [21]. It can be noted that at low carrier energy (e.g., <0.15 eV), the acoustic scattering dominates, while the optical scattering is more important at high kinetic energy

$$T_S = \frac{l_{\rm sc}(0)}{l_{\rm sc}(0)+L} \quad (27)$$

$$T_D = \frac{l_{\rm sc}(V_{\rm DSeff})}{l_{\rm sc}(V_{\rm DSeff})+L} \quad (28)$$

$$I_{{\rm DS}_p} = \frac{2qkT}{\pi\hbar}[T_S \ln(1+e^{E_F - qV_{\rm SC}/kT}) - T_D \ln(1+e^{E_F - q(V_{\rm SC}+V_{\rm DSeff})/kT})]. \quad (29)$$

Equations (27), (28), and (29) are to describe the scattering effects on the I–V characteristics. Fig. 6 illustrates that the phonon scattering effects may limit the transport capability of carriers in the channel, and hence, restrain the drain current. Different from (18), the scattering coefficients T_S and T_D are introduced in (29) that indicates the effects of the phonon scattering.

It can be seen from previous sections that some nonideal effects exist when operating a CNT transistor, and therefore, the transport characteristics becomes nonballistic. There can be quite a large number of factors including scattering mechanisms, parasitic capacitances, and energy barriers as well, and the transport phenomenons introduced before are just part of them. Some nonidealities, such as contact junction effects, are also of great importance. However, more theoretical analysis and mathematic expressions are needed before they can be added into the model. In reality, the nonballistic effects are caused by a number of factors, including fabrication technologies and materials, etc. Therefore, it becomes difficult to identify which effect is more important, and it can be seen that certain effects are dominant when the related coefficients are of great value in the provided device. For a model with nonballistic effects introduces before, the transport equation can be treated as the summary of the transport current and the tunneling current, which is also reflected in Fig. 2 as the parallel current sources.

By adding (21), (22), (25), and (29) to the original FETToy MATLAB scripts, we developed an extended model named FETToy+ [31] that has included the aforementioned four nonballistic effects in the model. Fig. 7 shows an accuracy comparison between FETToy and FETToy+ that combines the effects shown in Figs. 3–6, respectively.

V. Performance of Proposed Model

For an ideal model with no nonballistic effects, once the self-consistent voltage $V_{\rm SC}$ is efficiently calculated from the closed-form solutions of (8) after the approximation that yields only linear, quadratic, or a third-order polynomial relations, the total drain current can be directly obtained from (6), (7), and (18). However, when nonballistic transport features are considered, a more complicated model that includes additional coefficients and equations is needed. To clarify the distinction and compare the performance of the proposed models, separate simulations have been carried out for both ideal and nonballistic scenarios.

A. Ballistic Model

In the ballistic modeling approach, the calculations are extremely fast, as Newton–Raphson iterations and integration of

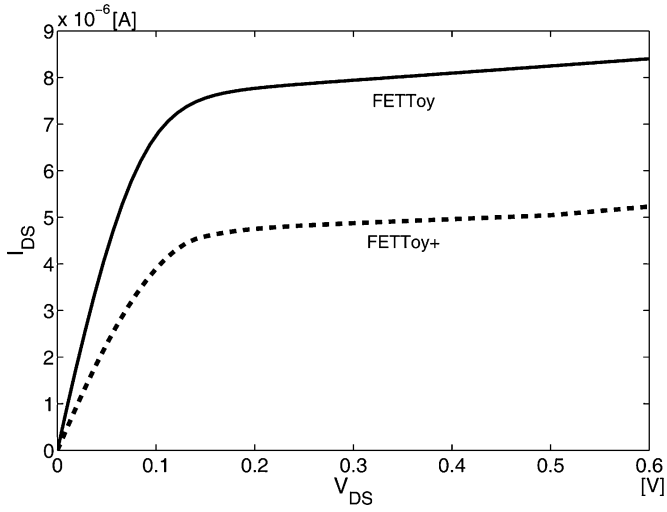

Fig. 7. Comparison of the drain currents at $V_G = 0.6$ V for FETToy (solid line) and FETToy+ (dashed line) models with 300 nm channel length and 1 nm diameter at $E_F = -0.32$ eV and $T = 300$ K.

TABLE I
COMPARISON OF AVERAGE CPU TIME AND MAXIMUM RMS ERROR OF PROPOSED BALLISTIC MODELS WITH FETTOY

FETToy CPU time	Spline model	Max RMSE	CPU time
1287 sec	**Model 1**	1.4%	11.7Sec
	Model 2	1.1%	19.3Sec

the Fermi–Dirac probability distribution are now eliminated. Table I shows the average CPU times for proposed models and FETToy. For accurate measurement, experiments were carried out by invoking all models 100 times. Results show that spline models are more than two orders of magnitude faster than FETToy. The extent to which the modeling accuracy was compromised by numerical approximation was also measured by calculating average rms errors in the simulations. Here, we chose the concept of normalized rms error, which is expressed as

$$\text{normalized RMSE} = \frac{\sqrt{\sum_{i=1}^{n}(a_i - b_i)^2/n}}{\max(a_i, b_i) - \min(a_i, b_i)}. \qquad (30)$$

Figs. 8 and 9 show the $I_{\rm DS}$ characteristics calculated by FETToy compared with two spline ballistic models, Model 1 and Model 2 using $n = 4$ and $n = 5$ points, respectively. As shown in Table I, both models maintain a high accuracy in terms of the average rms error. As expected, Model 2 is slightly more accurate with errors not exceeding 1.1% at $T = 300$ K and $E_F = -0.32$ eV throughout the typical ranges of drain voltages $V_{\rm DS}$ and gate bias V_G.

B. Models With Ballistic and Nonballistic Effects

When taking into account the nonballistic effects described in Section IV, the FETToy model [14], which implements the purely ballistic transport theory, cannot be used as a reference for accuracy and speed analysis. By adding (21), (22), (25), and (29) to the original FETToy MATLAB scripts, we developed

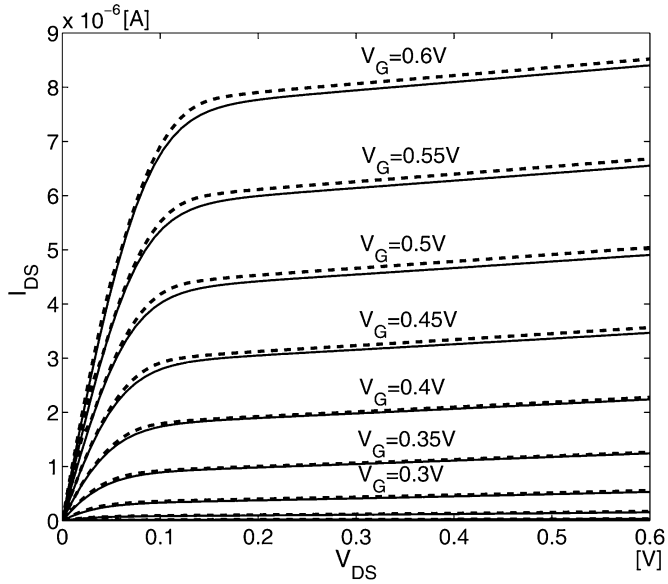

Fig. 8. Drain current characteristics at $T = 300$ K and $E_F = -0.32$ eV for FETToy(solid lines) and piecewise approximation using ballistic Model 1 (dashed lines).

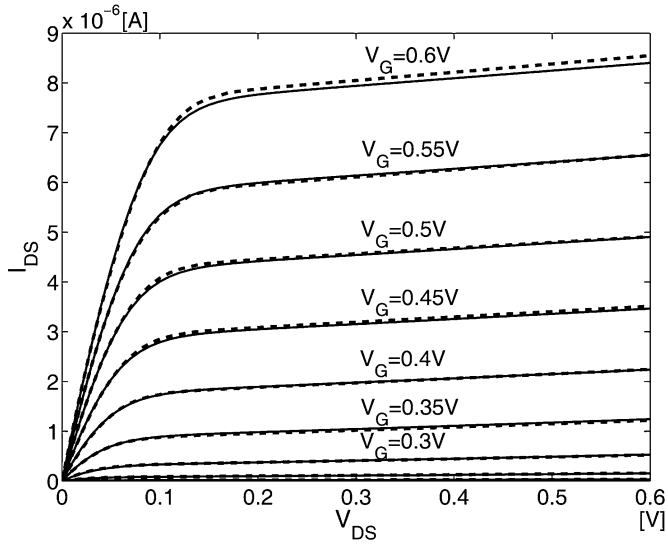

Fig. 9. Drain current characteristics at $T = 300$ K and $E_F = -0.32$ eV for FETToy (solid lines) and piecewise approximation using ballistic Model 2 (dashed lines).

an extended model named FETToy+ [31], which is capable of analyzing both ballistic and nonballistic performance of CNTs. Similarly, the cubic spline model has been enhanced to include the nonideal effects. The second group of simulations illustrate that the drain current may be reduced dramatically due to the presence of nonballistic effects. We have tested two spline-based nonballistic models, Models 3 and 4 with $n = 4$ and $n = 5$ spline points, respectively. Figs. 10 and 11 show the simulation results for FETToy+ and both the spline nonballistic models. In addition, the accuracy and the speed of the proposed models have been measured and compared with those of FETToy+, and results are listed in Table II. It can also be seen that the

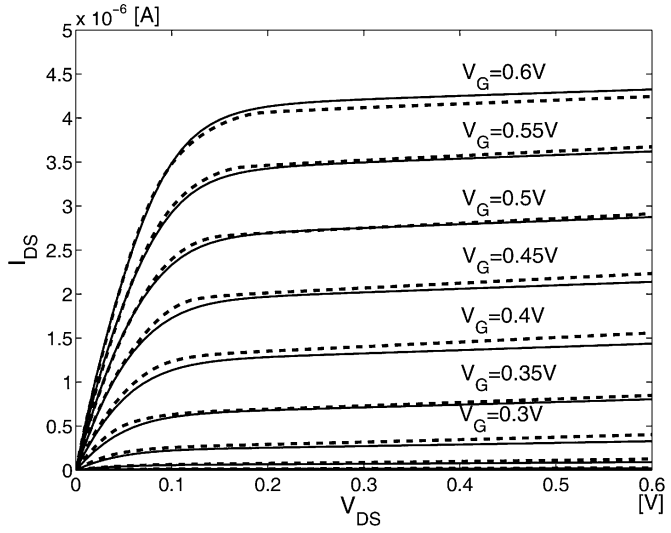

Fig. 10. Drain current characteristics at $T = 300$ K and $E_F = -0.32$ eV for a L $= 300$ nm CNT channel including nonballistic effects for FETToy + (solid lines) and piecewise approximation using nonballistic Model 3 (dashed lines).

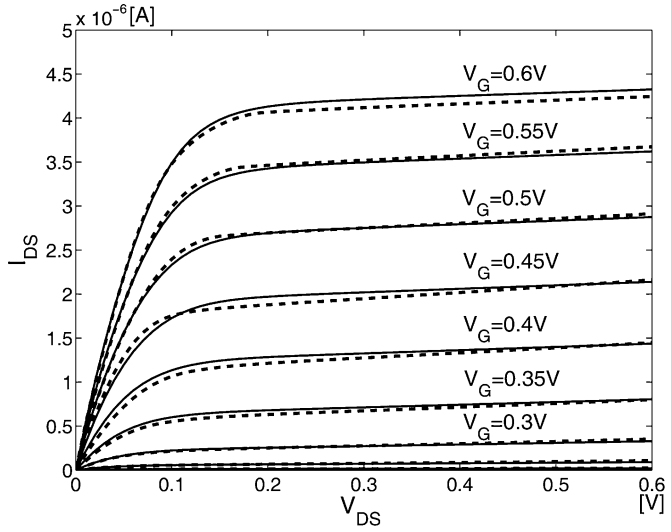

Fig. 11. Drain current characteristics at $T = 300$ K and $E_F = -0.32$ eV for a $L = 300$-nm-CNT channel including nonballistic effects for FETToy+(solid lines) and piecewise approximation using nonballistic Model 4 (dashed lines).

TABLE II
MAXIMUM RMS ERROR TO FETTOY+ AND AVERAGE CPU TIMES OF SPLINE MODELS WITH NONBALLISTIC EFFECTS

FETToy+ CPU time	**Spline model**	**Max RMSE**	**CPU time**
2261 sec	**Model 3**	1.9%	13.4 sec
	Model 4	1.5%	22.8Sec

nonballistic models consume more CPU time than ballistic models due to more complicated calculations.

VI. COMPARISON WITH EXPERIMENTAL RESULTS

Additionally, to validate the performance of the proposed models, some reported experimental characteristics were compared with the simulation results for $d = 1.6$ nm, $t_{\rm ox} = 50$ nm, $T = 300$, and $E_F = -0.05$ eV. Fig. 12 shows that the proposed cubic spline model with nonidealities obtains drain current performance close to the experimental measurements that were derived recently, and provided sufficient information about the transistor parameters [32]. The n-type CNT transistor was fabricated with K-doping and grounded back gate in the reported experiment. Table III shows the corresponding average normalized rms errors. As it can be seen from the following table and figure, both models maintain high accuracy over a wide-range temperature and Fermi level values for different CNT diameters with the nonballistic Model 4 being slightly mode-accurate.

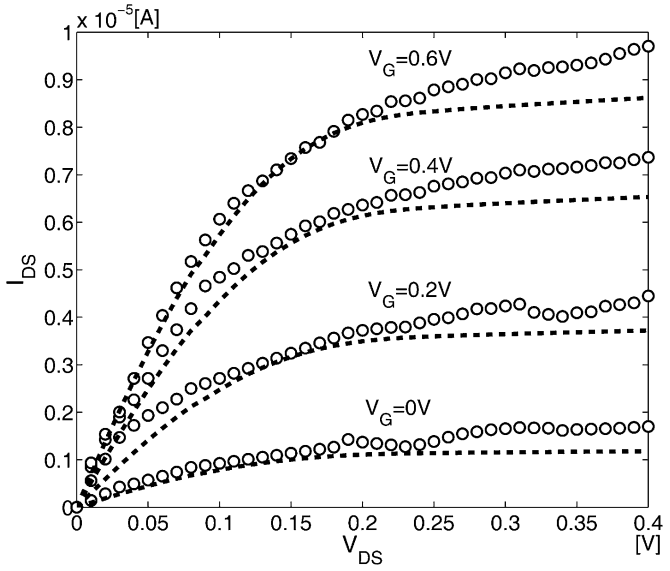

Fig. 12. Comparison to the experimental results(circlet lines) of the proposed nonballistic Model 4 (dashed lines) for $d = 1.6$ nm, $t_{\rm ox} = 50$ nm, $T = 300$ K, and $E_F = -0.05$ eV.

TABLE III
AVERAGE RMS ERRORS IN $I_{\rm DS}$ COMPARISON TO THE EXPERIMENTAL RESULTS OF FETTOY MODEL AND THE PROPOSED NONBALLISTIC (NB) MODELS FOR $d = 1.6$ NM, $t_{\rm ox} = 50$ NM, $T = 300$, AND $E_F = -0.05$ EV

$V_G[V]$	**Spline Model 3**	**Spline Model 4**
0.2	13.3%	12.8%
0.4	12.5%	11.9%
0.6	11.3%	10.6%

VII. CONCLUSION

A fast and efficient numerical approach to CNT transistor modeling has been proposed. It allows a straightforward incorporation of both ballistic and nonballistic transport effects. Results have shown that CPU times can be accelerated by two, or in some cases three, orders of magnitude compared with the traditional approach where time-consuming Fermi–Dirac integral and Newton–Raphson iterations are used. The key advantage of the presented technique is that it overcomes numerical difficulties in the calculation of the drain–source current by allowing a closed-form solution of the self-consistent voltage equation. Numerical integration and Newton–Raphson iterations are,

therefore, avoided, leading to a substantial acceleration in the model evaluation. The presented model concerns ballistic and nonballistic transport in the CNT itself. Future work involves the development of an enhanced CNT transistor model by adding effects external to the inner CNT transistor, such as the Schottky barrier between the CNT and metal contacts, multiple CNTs at a single gate, channel fringe capacitances, parasitic source/drain resistance, and series resistance due to the scattering effects.

ACKNOWLEDGMENT

The authors would like to thank the reviewers for their detailed and constructive comments on the manuscript that helped to improve the paper.

REFERENCES

[1] A. Rahman, J. Guo, S. Datta, and M. S. Lundstrom, "Theory of ballistic nanotransistors," *IEEE. Trans. Electron Devices*, vol. 50, no. 9, pp. 1853–1864, Sep. 2003.

[2] P. Avouris, J. Appenzeller, R. Martel, and S. J. Wind, "Carbon nanotube electronics," *Proc. IEEE*, vol. 91, no. 11, pp. 1772–1784, Nov. 2003.

[3] A. Raychodhury and K. Roy, "Carbon nanotube electronics: Design of high-performance and low-power digital circuits," *IEEE Trans. Circuits Syst.—I: Fundam. Theory Appl.*, vol. 54, no. 11, pp. 2391–2401, Nov. 2007.

[4] A. Raychowdhury, S. Mukhopadhyay, and K. Roy, "A circuit-compatible model of ballistic carbon nanotube field-effect transistors," *Appl. Phys. Lett.*, vol. 23, no. 10, pp. 1411–1420, Oct. 2004.

[5] B. C. Paul, S. Fujita, M. Okajima, and T. Lee, "Modeling and analysis of circuit performance of ballistic CNFET," presented at the 2006 Design Autom. Conf., San Francisco, CA, Jul. 24–28.

[6] J. Deng and H.-S. P. Wong, "A circuit-compatible SPICE model for enhancement mode carbon nanotube field effect transistors," presented at the 2006 Int. Conf. Simul. Semicond. Processes Devices, Piscataway, NJ, Sep. 6–8.

[7] K. Natori, Y. Kimura, and T. Shimizu, "Characteristics of a carbon nanotube field-effect transistor analyzed as a ballistic nanowire field-effect transistor," *J. Appl. Phys.*, vol. 97, no. 3, pp. 034306-1–034306-7, Feb. 2005.

[8] H. Hashempour and F. Lombardi, "An efficient and symbolic model for charge densities in ballistic carbon nanotube FETs," in *Proc. IEEE-NANO*, 2006, vol. 1, pp. 17–20.

[9] S. Hasan, S. Salahuddin, M. Vaidyanathan, and M. A. Alam, "High-frequency performance projections for ballistic carbon-nanotube transistors," *IEEE. Trans. Nanotechnol.*, vol. 5, no. 1, pp. 14–22, Jan. 2006.

[10] F. Leonard and D. A. Stewart, "Properties of short channel ballistic carbon nanotube transistors with ohmic contacts," *IEEE Trans. Nanotechnol.*, vol. 17, no. 18, pp. 4699–4705, Sep. 2006.

[11] J. Deng and H.-S. Philip Wong, "A compact spice model for carbon-nanotube field-effect transistors including nonidealities and its application—Part I: Model of the intrinsic channel region," *IEEE Trans. Electron Devices*, vol. 54, no. 12, pp. 3186–3194, Dec. 2007.

[12] J. Deng and H.-S. P. Wong, "A compact spice model for carbon-nanotube field-effect transistors including nonidealities and its application-Part II: Full device model and circuit performance benchmarking," *IEEE Trans. Electron Devices*, vol. 54, no. 12, pp. 3195–3205, Dec. 2007.

[13] Z. Chen, J. Appenzeller, Y.-M. Lin, J. Sippel Oakley, A. G. Rinzler, J. Tang, S. J. Wind, P. M. Solomon, and P. Avouris, "An integrated logic circuit assembled on a single carbon nanotube," *Science*, vol. 311, no. 5768, pp. 1735–1740, Mar. 2006.

[14] A. Rahman, J. Wang, J. Guo, S. Hasan, Y. Liu, A. Matsudaira, S. S. Ahmed, S. Datta, and M. Lundstrom. (2006, Feb. 14). Fettoy 2.0—On line tool [Online]. Available: https://www.nanohub.org/resources/220.

[15] T. J. Kazmierski, D. Zhou, and B. M. Al Hashimi, "A fast, numerical circuit-level model of carbon nanotube transistor," in *Proc. IEEE Int. Workshop Des. Test Defect-Tolerant Nanoscale Archit. (Nanoarch)*, Santa Clara, CA, Oct. 21–22, 2007, pp. 33–37.

[16] T. J. Kazmierski, D. Zhou, and B. M. Al Hashimi, "Efficient circuit-level modelling of ballistic CNT using piecewise non-linear approximation of mobile charge density," in *Proc. IEEE Int. conf. Des., Autom. Test Eur. (DATE)*, Munich, Germany, Mar. 10–14, 2008, pp. 146–151.

[17] J.-C. Charlier, X. Blase, and S. Roche, "Electronic and transport properties of nanotubes," *Rev. Modern Phys.*, vol. 79, no. 2, pp. 677–732, 2007.

[18] F. Liu, K. L. Wang, C. Li, and C. Zhou, "Study of random telegraph signals in single-walled carbon nanotube field effect transistors," *IEEE Trans. Nanotechnol.*, vol. 5, no. 5, pp. 441–445, Sep. 2006.

[19] A. Kanda, K. Tsukagoshi, Y. Aoyagi, and Y. Ootuka, "Gate-voltage dependence of zero-bias anomalies in multiwall carbon nanotubes," *Phys. Rev. Lett.*, vol. 92, no. 3, pp. 036801-1–036801-4, 2004.

[20] J. Guo and M. S. Lundstrom, "Role of phonon scattering in carbon nanotube field-effect transistors," *Appl. Phys. Lett.*, vol. 86, pp. 193103-1–193103-3, 2005.

[21] A. Balijepalli, S. Sinha, Y. Cao, "Compact modeling of carbon nanotube transistor for early stage process-design exploration," presented at the 2007 Int. Symp. Low Power Electron. Des. (ISLPED'07), Portland, OR, Aug. 27–29.

[22] M.-H. Yang, K. B. K. Teo, L. Gangloff, W. I. Milne, D. G. Hasko, Y. Robert, and P. Legagneux, "Advantages of top-gate, high-k dielectric carbon nanotube field-effect transistors," *Appl. Phys. Lett.*, vol. 88, no. 11, pp. 113507-1–113507-3, Mar. 2006.

[23] P. L. McEuen, M. S. Fuhrer, and H. Park, "Single-walled carbon nanotube electronics," *IEEE Trans. Nanotechnol.*, vol. 1, no. 1, pp. 78–845, Mar. 2002.

[24] J. Deng and H.-S. P. Wong, "Modeling and analysis of planar-gate electrostatic capacitance of 1-D FET with multiple cylindrical conducting channels," *IEEE Trans. Electron Devices*, vol. 54, no. 9, pp. 2377–2385, Sep. 2007.

[25] A. H. Carter, *Classical and Statistical Thermodynamics*. Redwood City, CA: Benjamin Cummings, May 2000.

[26] J. H. Mathews. (2005). Numerical analysis—Numerical methods [Online]. Available: http://math.fullerton.edu/mathews/numerical.html

[27] C. T. White and T. N. Todorov, "Carbon nanotubes as long ballistic conductors," *Nature*, vol. 393, pp. 240–242, 1998.

[28] J. Jiang, J. Dong, H. T. Yang, and D. Y. Xing, "Universal expression for localization length in metallic carbon nanotubes," *Phys. Rev. B*, vol. 64, pp. 045409-1–045409-4, 2001.

[29] I. Amlani, J. Lewis, K. Lee, R. Zhang, J. Deng, and H.-S. P. Wong, "First demonstration of ac gain from a single-walled carbon nanotube common-source amplifier," in *Proc. Electron Devices Meeting, (IEDM 2006) Int.*, Dec. 11–13, pp. 559–562.

[30] E. D. Minot, Y. Yaish, V. Sazonova, J.-Y. Park, M. Brink, and P. L. McEuen, "Tuning carbon nanotube band gaps with strain," *Phys. Rev. Lett.*, vol. 90, no. 15, pp. 156401/1–156401/14, Apr. 2003.

[31] D. Zhou, T. J. Kazmierski, B. M. Al Hashimi, P. Ashburn. (2008, Aug. 6). Southampton CNT resources [Online]. Available: https://www.cnt.ecs.soton.ac.uk

[32] A. Javey, R. Tu, D. Farmer, J. Guo, R. Gordon, and H. Dai1, "High performance n-type carbon nanotube field-effect transistors with chemically doped contacts,," *Nano Lett.*, vol. 5, pp. 345–348, 2005.

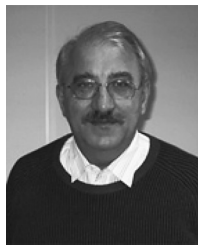

Tom Kazmierski (M'95) received the M.Sc. degree in electronic engineering in 1973 from Warsaw University of Technology, Warsaw, Poland, and the Ph.D. degree in 1976 from the Military Academy of Technology, Warsaw University of Technology.

Since 1984, he has been with the Department of Electronics and Computer Science, University of Southampton, Southampton, U.K., where he is currently engaged in the research of numerical modeling, simulation, and synthesis techniques for computer-aided design of very large-scale integration (VLSI) circuits. From 1990 to 1991, he was a Visiting Research Scientist at IBM VLSI Technology Division, San Jose, CA, where he developed and patented synchronization techniques for multisolver simulation backplanes. He has authored or coauthored more than 100 papers, and given a number of invited talks and tutorials mostly in the area of analogue and mixed-signal synthesis and hardware description languages. His current research interests include Web-based electronic design frameworks and applications of very high-speed integrated circuits (VHDL) analog and mixed-signal extension (AMS) to high-level system modeling and synthesis, involving modeling of mixed-domain systems, automated analogue and mixed-signal synthesis for application-specific integrated circuit (ASIC) design, including synthesis of artificial, VLSI neural networks.

Dr. Kazmierski has contributed to the development of the VHDL-AMS Standard by the IEEE. From 1999 to 2005, he was the Chair of the IEEE Design Automation Standards Committee (DASC) P1076.1 (VHDL-AMS) Working Group (WG), where he is currently the P1076.1 WG Secretary.

Dafeng Zhou received the B.Sc. degree in microelectronics in 2005 from Fudan University, Shanghai, China, and the M.Sc. degree in microelectronic design in 2006 from the University of Southampton, Southampton, U.K., where he is currently working toward the Ph.D. degree. His current research interests include circuit-level modeling and simulation of carbon nanotube devices.

Bashir M. Al-Hashimi (M'99–SM'01–F'09) received the B.Sc. degree (with first class) in electrical and electronics engineering from the University of Bath, Bath, U.K., in 1984, and the Ph.D. degree from York University, York, U.K., in 1989.

He was with the microelectronics design industry. In 1999, he joined the School of Electronics and Computer Science, Southampton University, where he is currently a Full Professor of computer engineering and the Director of the Pervasive System Center. He has authored one book on *SPICE Simulation* (CRC Press, 1995), and coauthored two books *Power Constrained Testing of VLSI Circuits* (Springer, 2002) and *System-Level Design Techniques for Energy-Efficient Embedded Systems* (Springer, 2004). In 2006, he edited the book, *System-on-Chip: Next Generation Electronics* (IEE Press, 2006). He has authored or coauthored more than 240 papers published in journals and refereed conference proceedings, and supervised 25 Ph.D. thesis successfully. He is an Editor of the *Journal of Electronic Testing: Theory and Applications (JETTA)*. He is a member of the Editorial Board of the *Journal of Low Power Electronics* and *Journal of Embedded Computing*. His current research interests include low-power system-level design, system-on-chip test, and reliable nano design.

Prof. Al-Hashimi is a Fellow of the Institute of Electrical Engineering (IEE) and the British Computer Society (BCS). He is the Editor-in-Chief of the IEE Proceedings: Computers and Digital Techniques. He was the General Chair of the 11th IEEE European Test Symposium (U.K., 2006) and the Technical Programme Chair of Design Automation and Test in Europe (DATE) 2009 and the General Chair 2011. He has received the James Beausang Best Paper Award at the 2000 IEEE International Test Conference for a paper relating to low-power built-in self-testable (BIST) for register-transfer level (RTL) data paths, and one of his paper on test data compression has recently been selected for a Springer book featuring the most influential work over the ten years of the DATE Conference.

Peter Ashburn (M'89) was born in Rotherham, U.K., in 1950. He received the B.Sc. degree in electrical and electronic engineering and the Ph.D. degree from the University of Leeds, Leeds, U.K., in 1971 and 1974, respectively.

In 1974, he joined the Technical Staff of Philips Research Laboratories, where he was engaged in ion-implanted integrated circuit bipolar transistors, and electron lithography for submicrometer integrated circuits. In 1978, he joined as a Lecturer in the Department of Electronics and Computer Science, University of Southampton, Southampton, U.K., where he is currently is the Personal Chair in Nanoelectronics and has been engaged in polysilicon emitter bipolar transistors, high-speed bipolar and BiCMOS technologies, gate delay expressions for bipolar circuits, and the effects of fluorine in bipolar transistors. He has authored and coauthored more than 250 papers in the technical literature, many invited papers, and has authored or coauthored books on the design and realization of bipolar transistors in 1988 and on silicon germanium heterojunction bipolar transistors in 2003. His current research interests include ultimate CMOS devices, carbon nanotube FETs, and nanowire biosensors.